

Simulated Strong Ground Motions for the Great M 9.3 Sumatra–Andaman Earthquake of 26 December 2004

by M. B. Sørensen,* K. Atakan, and N. Pulido

Abstract On 26 December 2004, a devastating earthquake of M 9.3 occurred offshore northern Sumatra. Due to the size of this earthquake and the accompanying tsunami wave, disastrous consequences have been observed in several countries around the Indian Ocean. The tectonics in the region are characterized by the oblique, north-northeast-oriented subduction of the Indian–Australian plate under the Sunda microplate with a rate of 6–6.5 cm/yr. This oblique convergence results in strain partitioning, where the trench-perpendicular thrust faulting along the subducting slab accommodates the east–west component of the motion, whereas the north–south component of the motion is probably accommodated by the right-lateral strike-slip faulting along the Great Sumatran fault and the Mentawi fault. Source parameters of the 26 December 2004 event have been used for modeling the resulting ground motions in the nearby affected regions. Results give an insight on the importance of ground shaking in the total destruction of places like Banda Aceh, northern Sumatra, Indonesia. The modeling is performed for a multiasperity finite fault using a hybrid procedure combining deterministic modeling at low frequencies and semistochastic modeling at high frequencies. Results show that strong shaking was distributed over a large area including northwestern Sumatra and its offshore islands. In Banda Aceh, which experienced significant damage, bedrock velocities reached 60 cm/sec with duration of the shaking of ca. 150 sec. The largest ground motions occurred near the strongest asperities of the fault plane, where velocities of 200 cm/sec are modeled for bedrock conditions.

Introduction

The Sumatra region has experienced several destructive earthquakes in the past, which are controlled by the tectonic processes in a convergent plate margin along the Sumatra trench. The north-northeast-oriented motion of the Indian–Australian plate (with a velocity of approximately 6 cm/year) (Khan and Gudmundsson, 2005) gives rise to an oblique collision that results in strain partitioning (McCaffrey *et al.*, 2000; Simoes *et al.*, 2004). The trench-perpendicular (ca. northeast–southwest) component of this motion is accommodated by the pure thrust earthquakes that take place along the coupled plate interface between the subducting Indian–Australian and the overriding Sunda plates. The shallow angle of subduction along this interface allows considerable stress accumulation and it is therefore capable of generating large thrust earthquakes. Such earthquakes were already considered in seismic hazard assessment for the region (Petersen *et al.*, 2004). Occurrence of the megathrust earthquakes ($M > 9$), however, were not observed until the 26

December 2004 Sumatra–Andaman earthquake (M_w 9.3). The trench-parallel component of the plate motion is accommodated by large strike-slip earthquakes that occur along the two parallel strands of faults, the Great Sumatran fault that lies parallel to the western coast of mainland Sumatra and its offshore equivalent the Mentawi fault (Prawirodirdjo *et al.*, 1997; McCaffrey *et al.*, 2000; Bilham, 2005).

The geometry of the subducting plate along the Sumatra–Andaman subduction zone varies along the trench. The obvious change of the trench orientation from south to north controls the distribution of the earthquakes that form an arclike structure (Fig. 1). The subduction plate interface as expressed by the earthquake distribution is wider in the south than in the north and there seems to be a marked change at around 10° N. This coincides with a location where the epicentral distribution of the seismicity splits into two main lines, one parallel to the trench and another one toward the Andaman Sea where it forms a rift associated with a backarc spreading (e.g., Eguchi *et al.*, 1979; Banghar, 1987; Ortiz and Bilham, 2003). The hypocentral depth distribution of instrumental seismicity reveals that the dip of the down-

*Present address: GeoForschungsZentrum Potsdam, Section 5.3, Telegrafenberg, 14473 Potsdam, Germany; sorenson@gfz-potsdam.de.

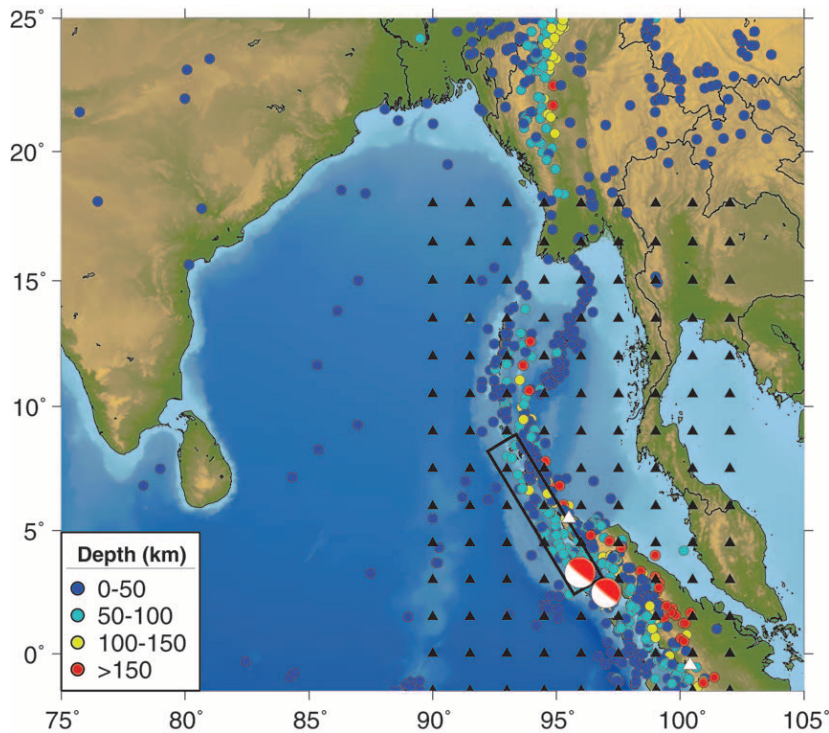


Figure 1. The region around the Indian Ocean including topography and bathymetry from the GEBCO database (Intergovernmental Oceanic Commission [IOC], International Hydrographic Organisation [IHO], and British Oceanographic Data Centre [BODC], 2003). Colored dots show earthquakes with $M > 5$ from the International Seismological Center (ISC) database for the time period 1900–1999 with the colors indicating the event depths. The red focal mechanisms show the 26 December 2004 and 28 March 2005 earthquakes with mechanisms from the Harvard CMT database. The black box shows the outline of the fault plane used for the ground-motion simulations, and black triangles show the simulation grid. The Banda Aceh and PPI sites are marked with white triangles.

going plate is relatively low (around 10°) at shallower depths (less than 30 km). With increasing depth, the dip becomes steeper and may be as steep as $40\text{--}45^\circ$. The maximum depth of the earthquakes range between 150 and 300 km and seems to gradually increase from 150 km in the north (at around 13° N) to almost 300 km in the south (at around 4° N).

Prior to the 26 December 2004 earthquake and the accompanying tsunami, there have been several large ($M > 8$) destructive and tsunamigenic thrust earthquakes in the history. The most significant of these are the 1797 (M 8.4), 1833 (M 9.0), and 1861 (M 8.5) earthquakes that occurred south of the 26 December 2004 earthquake rupture (Bilham, 2005; Lay *et al.*, 2005), whereas there have also been a few significant earthquakes with slightly smaller size along the Nicobar (M 7.9) and Andaman (M 7.7) islands regions in 1881 (Ortiz and Bilham, 2003) and 1941, respectively. Occurrence of these large earthquakes are typical both in size and frequency for the Java–Sumatra subduction zone. However, the 26 December 2004 earthquake differed both in its enormous dimensions covering a total fault area of almost 1300 km along strike with variable width between 160 and 240 km, as well as in its slip characteristics.

Following the 26 December 2004 event, there was much focus on the possible implications of the static stress transfer on neighboring segments of the trench. Coulomb stress transfer modeling performed by McClosky *et al.* (2005), estimated positive stress changes along the southern part of the December rupture. These estimates were then manifested by the earthquake of 28 March 2005 (M 8.7) that occurred along the southern part of the Sumatra trench close to the island of Nias. The location and the size of this earthquake was

similar to the historical earthquake that occurred along the same segment in 1861. The 28 March earthquake was also a typical thrust event occurring along the plate interface between the subducting Indian–Australian plate in the southwest and the overriding Sunda plate in the northeast.

One of the main questions posed after the 26 December 2004 Sumatra–Andaman earthquake was related to the strong ground motion distribution in the region and its consequences in places like Banda Aceh where severe destruction was observed. Although much of the damage was associated with the accompanying tsunami, it is still not clear how much of the destruction was due to strong ground shaking. In the present study we therefore focus on the ground-motion distribution related to this megathrust earthquake. Since there were only a few strong-motion recording sites nearby we address this problem by simulating for broadband waveforms based on a hybrid methodology.

Ground-Motion Modeling Methodology

We follow the approach of Pulido and Kubo (2004) and Pulido *et al.* (2004), using a hybrid method for modeling the ground motions caused by the 26 December 2004 earthquake. This procedure combines a deterministic simulation at low frequencies (0.1–1 Hz) with a semistochastic simulation at high frequencies (1–10 Hz). Our scenario earthquake source input model includes a finite fault with asperities embedded in a flat-layered one-dimensional (1D) velocity structure. The source consists of a number of asperities, which are divided into subfaults assumed to be point sources. The total ground motion at a given site is obtained

by summing the contributions from the different subfaults. For the low frequencies, subfault contributions are calculated using discrete wavenumber theory (Bouchon, 1981) and summed assuming a given rupture velocity. At high frequencies, the subfault contributions are calculated using a stochastic method that incorporates a frequency-dependent radiation pattern by applying a smooth transition from a theoretical double-couple radiation pattern at low frequencies to a uniform radiation pattern at high frequencies following Pulido and Kubo (2004). Point sources are summed using the empirical Green's function method of Irikura (1986). The ground-motion simulations are performed at bedrock level and therefore do not take local site effects into account.

As input for the modeling, the source needs to be defined in terms of the location of the rupturing fault and its asperities together with asperity parameters such as rise time, rupture velocity, stress drop, and seismic moment. In addition, the properties of the surrounding crust need to be defined including the velocity structure and attenuation characteristics. Much of the information regarding the fault rupture characteristics is based on the available interpretations made by source inversion studies as discussed subsequently.

Source Model for the 26 December 2004 Sumatra–Andaman Megathrust Earthquake

The 26 December 2004 event started with a rupture at a latitude around 3° N along the Sunda trench with a depth of about 30 km. The rupture reached up to 20 m slip with fast velocities (ca 3 km/sec) for the first 420 km (Sumatra segment), then slowed down for the next 325 km (Nicobar segment) with an average rupture velocity of 2.5 km/sec and 5-m slip (Lay *et al.*, 2005). The remaining Andaman segment, which extends northward for about 570 km, had very slow slip with, on the average, less than 2-m displacements, distributed over a time segment from 600 up to 3500 sec. This has produced seismic signals and excited free oscillations of the earth that could be recorded with very long periods up to 20 min (Park *et al.*, 2005; Stein and Okal, 2005). The first 600 sec of the seismic signal consisted of the faster Sumatra segment rupture at the southern end of the fault which transitionally changed into a slower slip along the Nicobar segment. During this transition the width of the fault also narrowed down from 240 km to 170 km (Bilham, 2005; Lay *et al.*, 2005). The seismic moment (M_0) of the fast and the slower segments was 6.5×10^{22} N m and 3.0×10^{22} N m, respectively. In total the earthquake had a seismic energy (E_R) equivalent of 4.3×10^{18} J. (Ammon *et al.*, 2005; Bilham, 2005; Lay *et al.*, 2005).

There has been a number of source inversions made immediately after the 26 December 2004 earthquake was recorded on global seismic stations. Based on the teleseismic records and the inversion schemes used, different earthquake source-slip models have been obtained and presented. The most notable of these were the source inversions made by Ji (2005) and Yagi (2004). Extended versions of these results

(e.g., Ammon *et al.*, 2005; Lay *et al.*, 2005) are now used in both tsunami modeling (e.g., Glimsdal *et al.*, 2006) and in ground-motion simulations.

The main uncertainty with regard to the source concerns the slip distribution and the variation of rupture velocity along the entire fault length of 1300 km. The initial 420 km have been successfully modeled by both Ji (2005), Yamanaka (2005), and Yagi (2004); however, the northward extension of the fault and the transition from a fast to slow slip has been difficult to interpret with regard to the tsunami generation. The general consensus reached by several authors recently (e.g., Bilham, 2005; Ammon *et al.*, 2005; Lay *et al.*, 2005; Stein and Okal, 2005), agree on the rupture characteristics of the southernmost Sumatra segment with its fast slip. However, the transition from fast-to slow-slip along the Nicobar segment and the following extremely slow slip generated by the northernmost Andaman segment are poorly understood with respect to their contribution to the resulting tsunami. It is important to note here that the total energy released is tripled due to this slow slip component, from the initial estimates of M_W 9.0 to M_W 9.3. Although the slip was very slow, the geodetic data (Global Positioning System [GPS]) indicate permanent deformations in the order of several meters along the Andaman segment (Bilham, 2005).

Scenario Earthquake Parameters

The source parameters used in this study have been chosen among the large amount of published material on the 26 December 2004 earthquake. A summary of the parameters is given in Table 1.

As a general basis for the input model we used the source model published by Yagi (2004) shortly after the earthquake. This model has been obtained through *P*-wave inversion of data from 13 IRIS stations in the frequency range 4–200 sec. Due to the limited frequency band in the inversion, only the southernmost 660 km of the rupture is included in the model. We have modified this model following the results of Lay *et al.* (2005), extending the fault length

Table 1
Source Parameters Used in the Ground-Motion Simulations

Seismic moment	$M_0 = 6.5 \cdot 10^{22}$ N/m*
Fault-plane solution (strike/dip/rake)	$329^\circ/10^\circ/110^\circ$ †
Average stress drop	6.0 Mpa‡
Asperity stress drop (high slip)	10 Mpa‡
Asperity stress drop (intermediate slip)	35 Mpa‡
Rise time	6.0 ± 2 sec§
Rupture velocity	2.5 ± 0.5 km/sec¶
f_{\max}	10 Hz§
Q	$100 f^{0.88}$

*Fast-slip component of Lay *et al.*, (2005).

†Yagi (2004).

‡Following Pulido *et al.*, (2004).

§See text for discussion

¶Yagi; 2004; Ammon *et al.*, (2005).

to 750 km, thereby representing the Sumatra and Nicobar segments of their source model that are interpreted to be the only segments experiencing significant ($>2\text{m}$) fast slip. The fault width is kept constant at 150 km along dip for the entire fault as given by Yagi (2004).

The hypocenter of the earthquake is taken from the U.S. Geological Survey (USGS), which is also the hypocenter used by Yagi (2004). This hypocenter has a depth of 30 km, meaning that the uppermost edge of the rupturing fault plane is buried at 17-km depth. We use a seismic moment of $M_0 = 6.5 \times 10^{22}$ N m which is equal to the seismic moment released through fast slip on the Sumatra and Nicobar segments during the earthquake (Lay *et al.*, 2005). The fast-slip contribution of the Andaman segment of Lay *et al.* (2005) to the total seismic moment is negligible, since this is only ca 0.8% of the total seismic moment. We have not included slow slip in our computations, considering that this is not expected to contribute significantly to the ground shaking.

Among different authors there is a general agreement that the mechanism of the 26 December 2004 earthquake was almost pure thrust faulting. In our computations we have used the fault-plane solution given by Yagi (2004), which is very similar to the Harvard CMT solution.

Based on the slip model of Yagi (2004), a number of asperities have been defined on the ruptured fault plane. A comparison of the Yagi (2004) model and the input model geometry is shown in Figure 2. Due to the large variations in slip, two types of asperities have been defined with dif-

ferent asperity parameters. Asperities 1 and 2 comprise the regions of highest slip (ca. 10–20 m) and are referred to as high-slip asperities. Asperities 3–5 cover the regions of slip in the range ca. 5–10 m and are referred to as intermediate-slip asperities. Each class of asperities is defined with parameters characteristic for the given class. A map view of the input model including the asperities is shown on a bathymetry map of the area in Figure 3.

The stress drop has been calculated based on seismic moment and asperity area using the relationships of Das and Kostrov (1986) and Brune (1970) as described by Pulido *et al.* (2004). For the rupture velocity we use a value for the individual subfaults, varying randomly around 2.5 ± 0.5 km/sec. The average value of 2.5 km/sec is in agreement with the results of Yagi (2004) and Ammon *et al.* (2005), for example, and the random variation is included in order to take into account the natural variations in rupture velocity due to heterogeneities along the fault. A rise time varying randomly around 6 ± 2 sec has been used, which is estimated from past large earthquakes and scaled to leave time for the significant amount of slip occurring during the earthquake.

We have used a regional velocity model based on the results of Masturyono *et al.* (2001) who performed a tomographic inversion of travel-time data around the Toba caldera complex of northern Sumatra. Their regional average velocity model has been modified by adding a 2-km-thick low-velocity layer ($V_s = 1500$ m/sec) at the surface. The

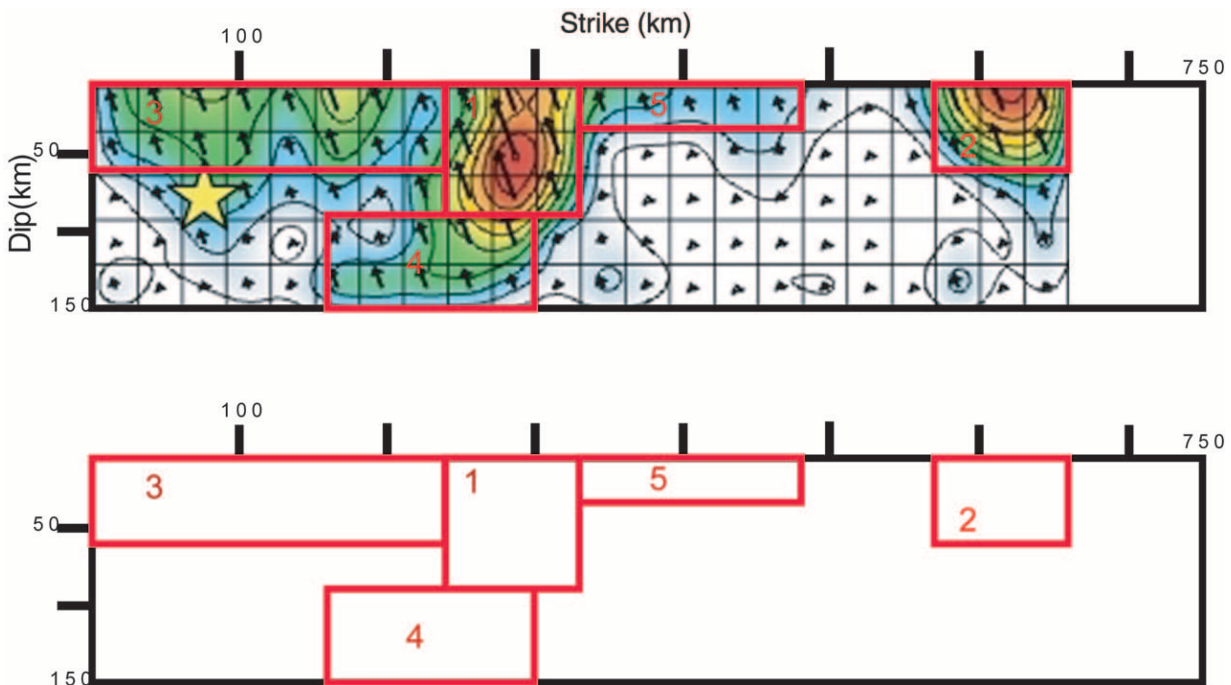


Figure 2. The geometry of the input source model compared to the Yagi (2004) model. The black box outlines the rupturing fault plane, the red boxes outline the asperities. Asperities 1 and 2 are high-slip asperities, 3–5 are intermediate-slip asperities. Modified from Yagi (2004).

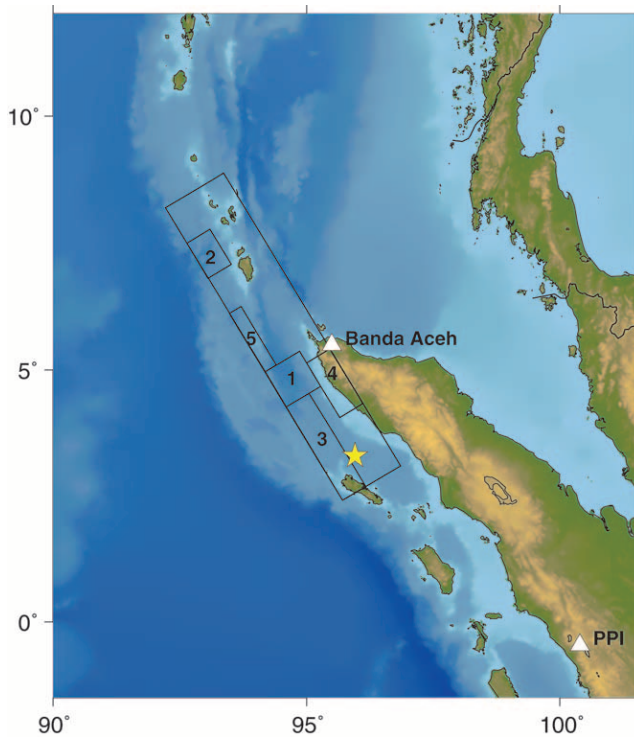


Figure 3. The location of the modeled fault plane. Topography and bathymetry data are from the GEBCO database (IOC, IHO, and BODC, 2003). The fault plane, which is dipping 10° , has been projected to the surface. Asperities are marked with the corresponding asperity number. Asperities 1 and 2 are high-slip asperities, and asperities 3–5 are intermediate-slip asperities. The star shows the surface projection of the hypocenter, the white triangles the Banda Aceh and PPI sites.

resulting model is shown in Figure 4. Little is known about the regional attenuation, and a general Q -relationship of $Q = 100f^{0.8}$ is used. The cutoff frequency f_{\max} , which is the frequency above which the acceleration spectrum decays rapidly, is set at a value of 10 Hz, which is also the upper frequency limit of our computations. In this respect, the high-frequency decay of ground motions is controlled only by the attenuation controlled by the Q factor.

Based on the aforementioned input scenario, ground-motion simulations were performed on a regular grid of 144 points with a grid spacing of 1.5° , located as shown in Figure 1. Furthermore, simulations were performed at the PPI-JISNET (Japan–Indonesia Broadband Seismic Network) station (Ishida *et al.* 1999), which is to our knowledge the closest seismic recording (650 km) of the 26 December 2004 Sumatra–Andaman mainshock. We also performed simulations at a site located at Banda Aceh (Fig. 1) in order to study the ground shaking at this location in more detail.

Due to the enormous size of the ruptured fault plane, the scenario computations are on the limit of what is feasible in terms of computation time, using the chosen ground-motion simulation methodology. We used a subfault dimen-

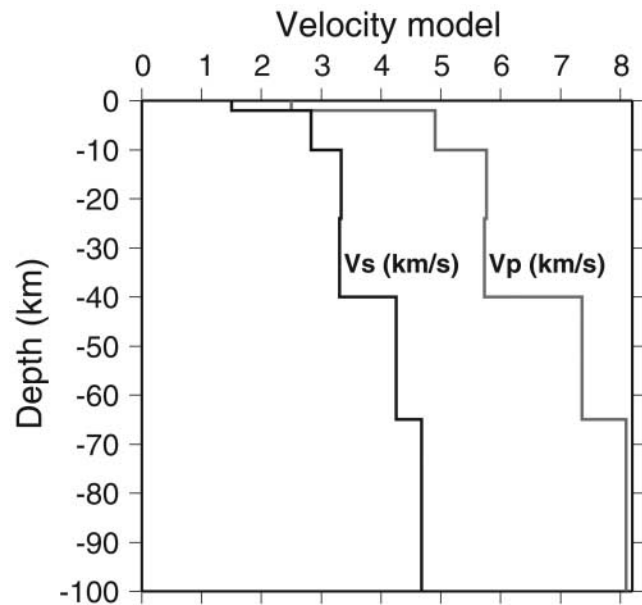


Figure 4. Crustal velocity structure of the Sumatra–Andaman region (based on Masturyono [2001] which has been modified for the upper 2 km).

sion of 10×10 km for the background slip and 5×5 km for the asperities. This was chosen as a trade-off between a reasonable resolution in the source model and manageable computation times.

Simulation Results

Our simulations provide waveforms for the ground motions at all the simulation sites for an outcrop bedrock condition. We retrieve the peak ground motions (PGA and PGV) to get an insight to the distribution and extent of the strong shaking. Figures 5 and 6 show the PGV and PGA distributions, respectively. From these figures it is clear that the strongest shaking occurs close to the rupturing fault plane and that the reverse mechanism of the earthquake has a strong effect on the directivity of the ground motions. PGV values reach up to 200 cm/sec above the fault plane and are strongest in the region near asperity 1. This is probably a combined effect of the large moment release and large size of this asperity and the proximity to the rupture initiation point. On land in northern Sumatra, velocities reach values up to 100 cm/sec at bedrock level. The PGA distribution differs significantly from the PGVs, and we observe significant PGAs (in the order of $0.5g$) over the entire fault plane. Additionally, the largest values of PGAs are predicted in the area around asperity 1 reaching values of 1200 cm/sec^2 , but also asperity 2 and the intermediate-slip asperities have a significant effect on the ground accelerations. This has an important implication for the Nicobar islands which have experienced significantly large accelerations. Largest bedrock accelerations on northern Sumatra are in the order of $0.4g$.

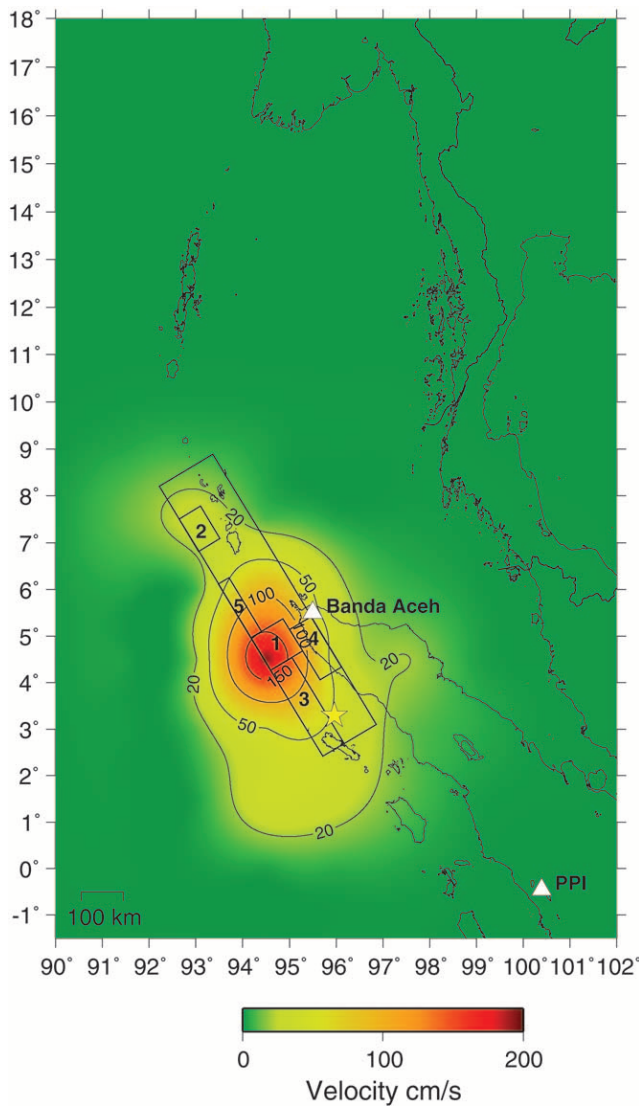


Figure 5. PGV distribution in the study area. The black boxes indicate the extent of the surface projection of the fault plane and its asperities. The star shows the surface projection of the hypocenter, and the white triangles indicate the Banda Aceh and PPI sites.

There is a strong correlation between the extent of the strong ground shaking and the extent of the rupturing fault plane (Fig. 5, 6), especially with respect to the distribution of strong accelerations (Fig. 6). It should be noted here that our simulations are based on a source model that does not include the northernmost segment where an average slip of 2 m was estimated (Lay *et al.*, 2005). Most of the slip in this area, however, was associated with the very slow slip and did probably not contribute to the strong ground motion distribution. As a consequence of this, extending the fault plane northward, and including the ca. 2 m of slip along the Andaman segment of Lay *et al.* (2005) would extend the area of significant shaking northward. It may be argued that this would provide unrealistically high ground-motion estimates

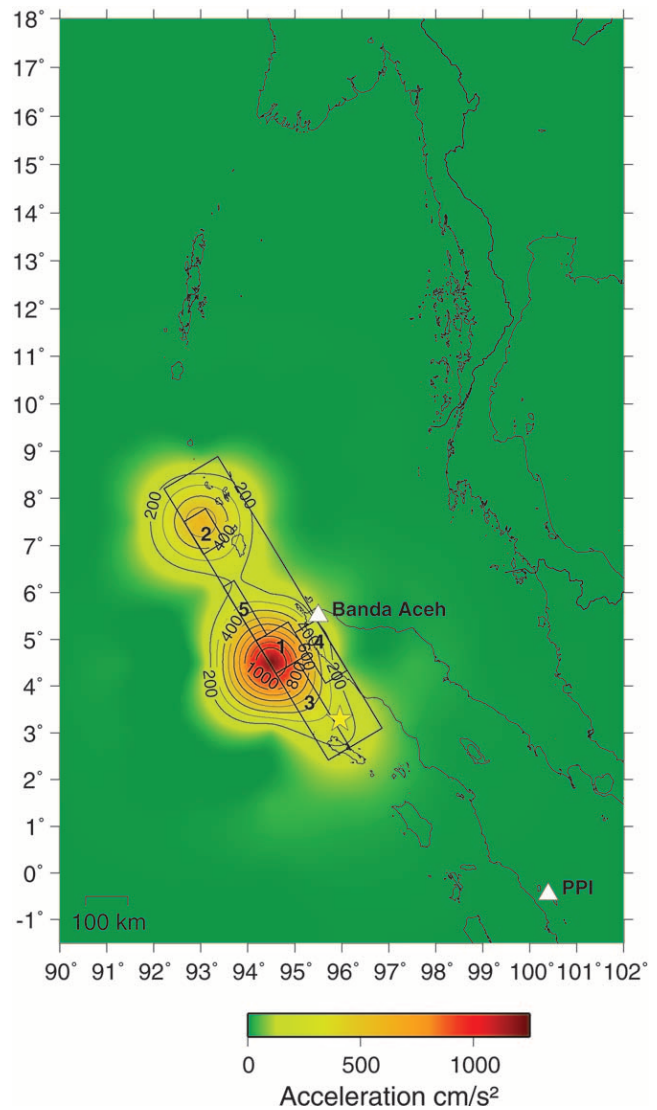


Figure 6. PGA distribution in the study area. The black boxes indicate the extent of the surface projection of the fault plane and its asperities. The star shows the surface projection of the hypocenter, and the white triangles indicate the Banda Aceh and PPI sites.

for the Andaman Islands. In any case, the rest of the region would be little affected since the distance from this segment to for example Myanmar, Thailand, or Sumatra is significantly larger and hence the released seismic energy would be attenuated along the propagated path. The same is observed for the energy released along the modeled fault segments that is almost completely attenuated along the path toward the Andaman Islands. This underlines an important property of the ground shaking caused by very large earthquakes. Due to the large extent of the fault planes for these earthquakes, a single point even close to the fault will not be affected by the entire amount of released energy due to attenuation occurring along the fault. Therefore there is an upper limit to the ground-shaking levels a given area can

experience, which is more dependent on the amount of slip along the fault segments close to (i.e., within a few hundred kilometers from) the site of interest than on the total magnitude of the earthquake.

Comparison with Observed Seismic Data

Few near-field recordings are available from the earthquake due to a lack of strong-motion stations in the region. To our knowledge, the nearest station recording the 26 December 2004 earthquake was the PPI station of the JISNET network (Ishida *et al.*, 1999) located approximately 650 km southeast from the earthquake hypocenter (Fig. 3). We have compared the recording from this station to simulations performed at the location of the station, filtered between 0.1 and 10 Hz (Fig. 7). The surface waves are dominating in the recorded waveform but are not well reproduced in our calculations for the ground motion, mainly because of our assumption of a simple one-dimensional (1D) velocity struc-

ture model. Therefore the main comparison should be made between the *S* waves of the signals. For the vertical component of the ground motion there is a good agreement between the amplitudes of the recorded and simulated *S* waves, and the timing of the *S*-wave onsets fit well. For the horizontal components, the synthetic waveforms underestimate the ground-motion levels by a factor of 2–3. The good match at the vertical components indicate that this discrepancy may be due to local site effects at the recording site, however other explanations such as uncertainties in the attenuation model cannot be excluded. The duration of the simulated *S* waves seem also to agree well with the recorded data (most clearly seen for the vertical component), but an extended part of the *S*-wave energy due to for example local site effects may be hidden in the surface waves.

To test how well the frequency content of the ground motion is simulated, we show in Figure 8a a comparison between the recorded and simulated spectral velocities at the PPI station. It is interesting to observe that the recorded spec-

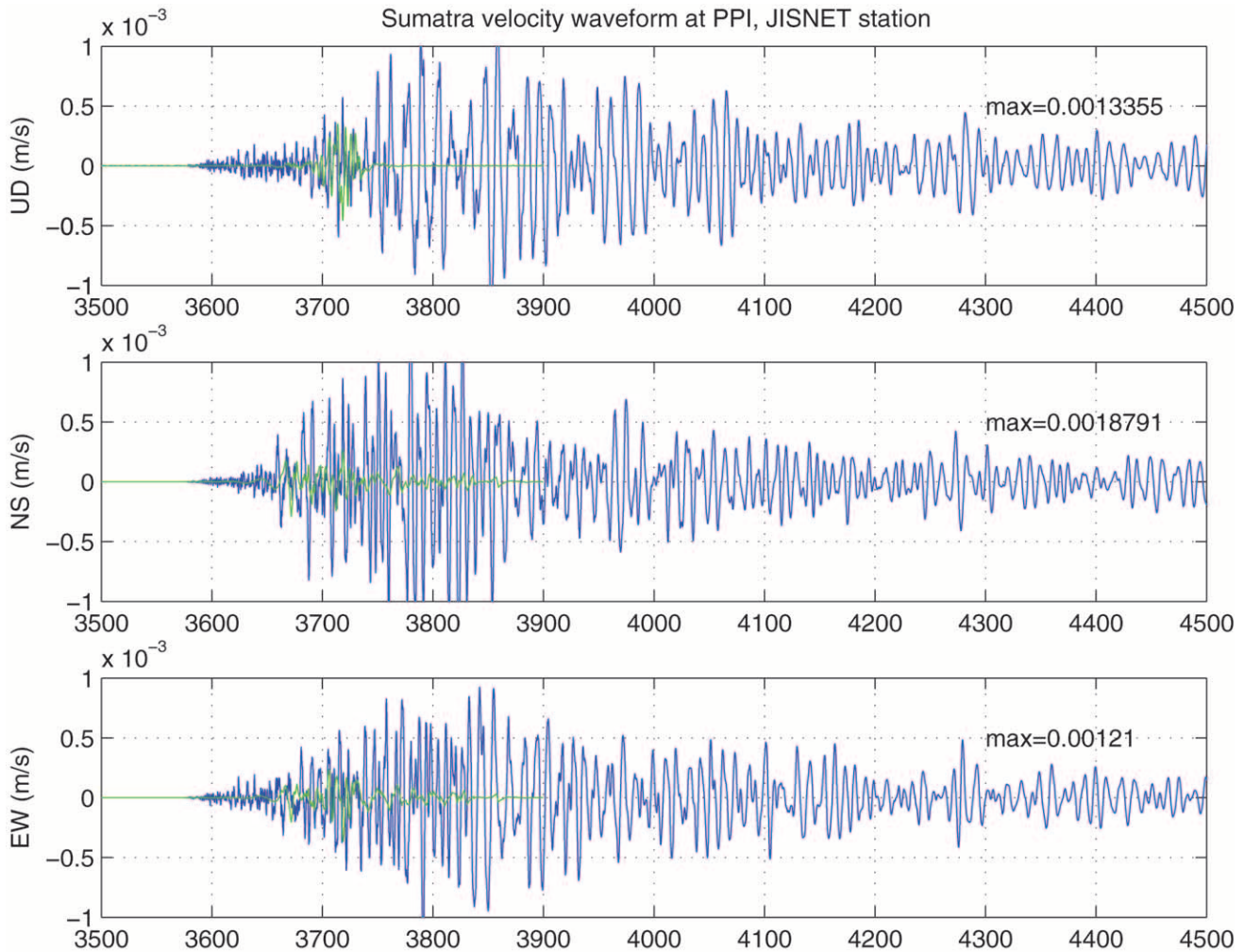


Figure 7. Comparison between recorded (blue) and simulated (green) velocity waveforms for the PPI station of the JISNET network. The horizontal scale is time in seconds after the origin time.

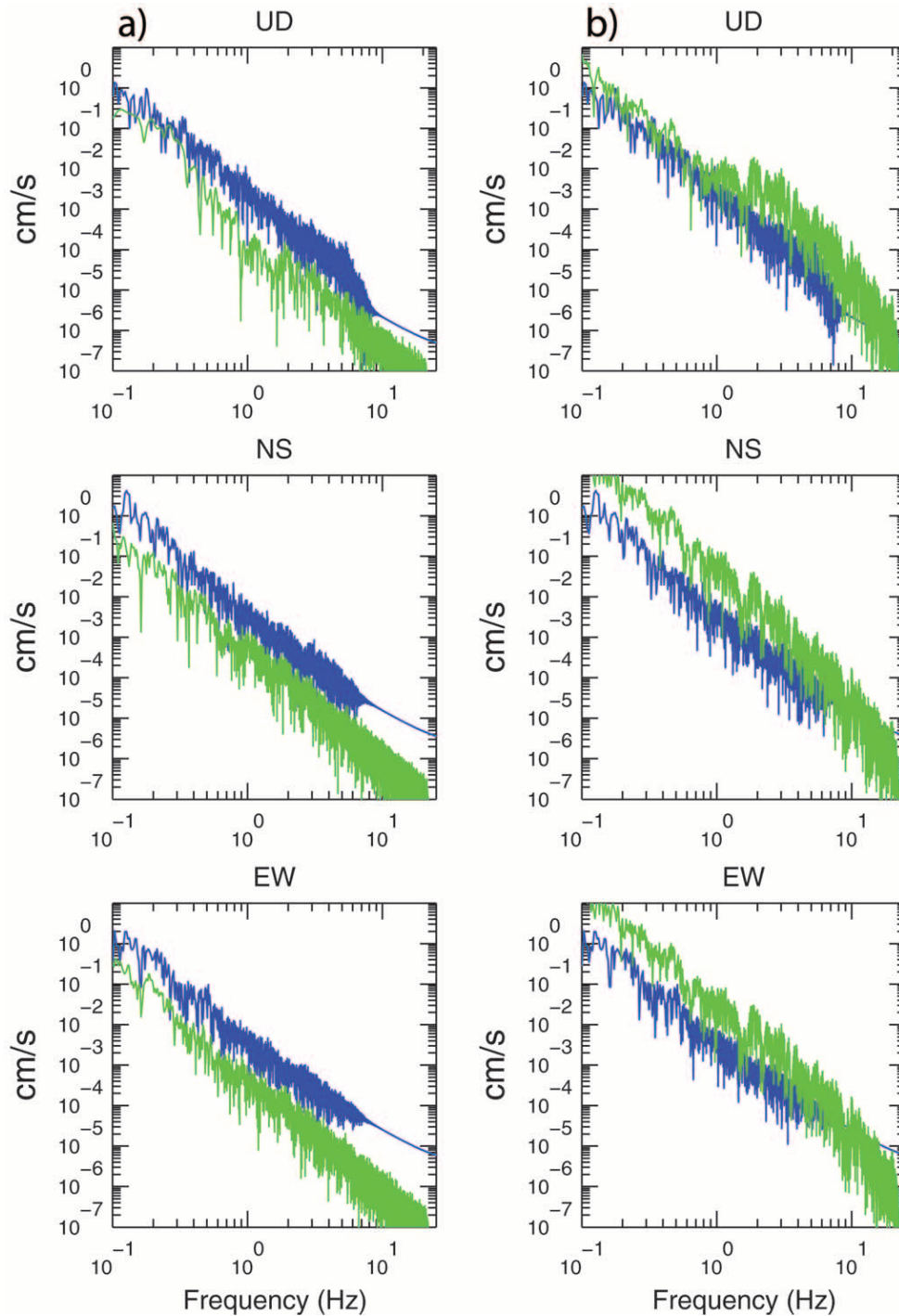


Figure 8. Comparison between spectra of recorded (blue) and simulated (green) velocity waveforms for the PPI station of the JISNET network (a) Simulated waveform is calculated using a $1/R$ geometrical spreading function; (b) simulated waveform is calculated using a $1/R^{0.5}$ geometrical spreading function.

tra approximately follow an ω^2 -model despite the enormous size of the earthquake. Also, our simulations do a good job in reproducing this ω^2 -model. There is a difference between the absolute levels of the spectra where our simulations slightly underestimate the observed spectra. As discussed

previously, this may be an effect of the local geology; however, other factors may also contribute to this underestimation. First, our high-frequency computations do not take into account scattering of the seismic waves as they propagate through the heterogeneous complex media. This may in re-

ality be a significant contribution to the observed energy and can explain some of the mismatch. Secondly, we are assuming a $1/R$ geometrical spreading in our computations. Several authors suggest a geometrical spreading proportional to $1/R^{0.5}$ at large distances (e.g., Boore, 2003). In Figure 8b, the spectrum has been calculated for a waveform simulated using a geometrical spreading proportional to $1/R^{0.5}$ for $R > 130$ km (used by, e.g., Atkinson and Boore [1995] for eastern North America). This provides a better fit to the absolute ground-motion levels that are, however, slightly over-estimated.

In Figure 9, a comparison has been made between the simulated PGA and PGV values at simulated sites with distances less than 500 km to asperity 1 and ground motions predicted by a number of empirical attenuation relationships. Recordings at larger distances than 500 km are expected to be dominated by surface waves that are not well reproduced in our simulations. Also included in the plot are peak ground motions recorded at 10 stations of the global digital seismographic network (GDSN) in India as reported by Singh *et al.* (2005). For each site the peak ground motion has been plotted against the minimum distance to asperity 1. As seen in the figure there is reasonably good agreement between the simulated ground motions and empirical predictions, despite the limited magnitude range used in determining the empirical relations and the uncertainty in distance due to the dimensions of the fault plane. There is a general tendency at the shorter distances of PGA lying below the attenuation curves and PGV being higher than predicted by the attenuation relations for the simulated data. This tendency is confirmed by the recordings at the stations in India at much larger distances, indicating that the attenuation relations are uncertain at the large magnitude of the 26 December 2004 earthquake. At distances close to 500 km the ground motions fall off faster than predicted by the attenuation relations and indicated by the recorded data. This is probably due to a combination of the increased significance of surface waves at these distances and uncertainties in the attenuation relation used in the modeling.

Simulated Ground Motion in Banda Aceh

Figure 10 shows an example of a simulated seismogram for the Banda Aceh site. This site is located at a distance of ca. 100 km from the fault plane and is in this respect expected to experience strong shaking. This has also been confirmed by eyewitnesses (see, e.g., the online intensity map of the USGS http://pasadena.wr.usgs.gov/shake/ous/STORE/Xslav_04/ciim_display.html).

An earthquake damage survey in Banda Aceh by a Japanese team estimated the observed intensities based on 174 questionnaire responses to be as large as 6 on the Japan Meteorological Agency (JMA) scale, which corresponds approximately to an MM intensity of IX (Honda *et al.*, 2005). Applying empirical relations between peak ground motion and intensity gives correspondingly a PGA of approximately

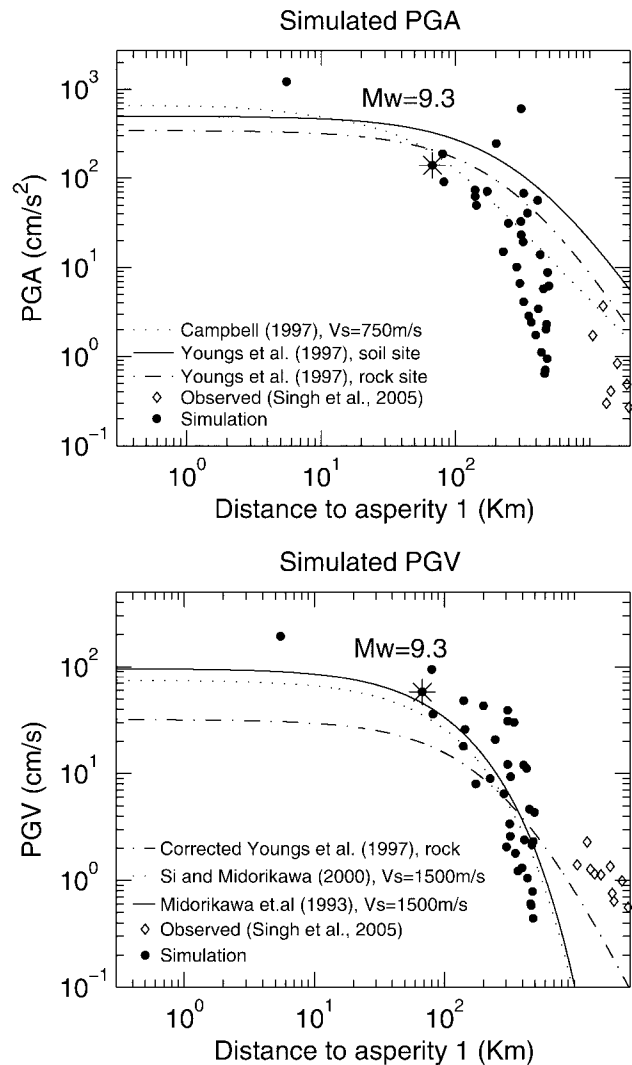


Figure 9. Comparison of simulated (black dots) and recorded (open diamonds, from Singh *et al.*, [2005]) PGA and PGV to ground motions predicted by empirical attenuation relations of Youngs *et al.* (1997) (for rock and soil site); and Campbell (1997) for PGA (uppermost plot); and Si and Midorikawa (2000), Midorikawa (1993), and a corrected version of Youngs *et al.* (1997) (rock site) applying the results of Newmark and Hall (1982) for PGV (lowermost plot). The star represents the Banda Aceh site (see Figs. 1 and 3 for location of the site).

300 cm/sec^2 (Murphy and O'Brien, 1977) or a PGV of approximately 80 cm/sec (Wald *et al.*, 1999). Our simulations indicate ground motions reaching acceleration levels of 140 cm/sec^2 and velocities up to 60 cm/sec at bedrock level. A comparison of the ground-motion values obtained by modeling and based on the intensities shows that we expect site amplifications in the order of a factor of 1.5–2. This is a reasonable estimate, considering that we are dealing with strong ground motion in an area where local site effects are expected to be significant. Similar levels of amplification have been estimated for the city of Istanbul, Turkey, based

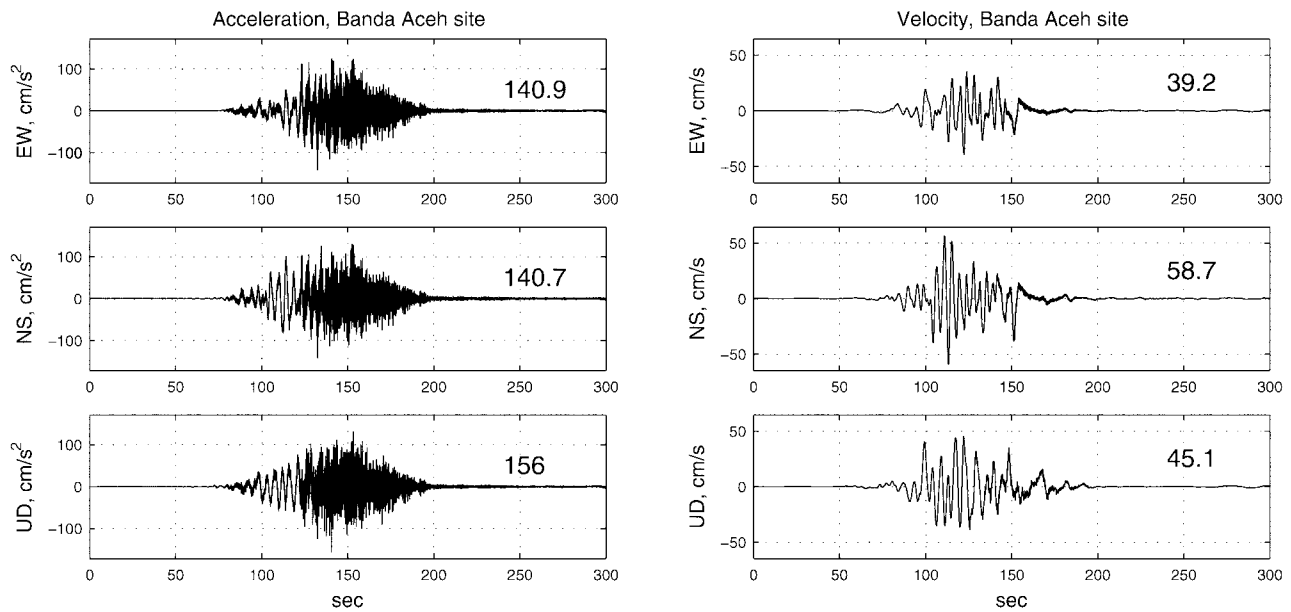


Figure 10. Acceleration (left) and velocity (right) waveforms for the simulation point located in Banda Aceh, northern Sumatra (see Figs. 1 and 3 for location of the site). The numbers to the right above the traces give the peak ground-motion values.

on modeling of strong ground motion (Sørensen *et al.*, 2006), however, much more details about the geological and geotechnical conditions are needed before similar studies can be carried out for Banda Aceh. Another important information given by the simulated waveforms is the duration of the ground shaking that has a significant impact on the resulting damage. From the waveforms in Figure 10 it is seen that shaking in Banda Aceh lasted for approximately 150 sec while the strongest shaking continued for more than 1 min.

Figure 11 shows pseudoacceleration response spectra with 5% damping for the 26 December 2004 earthquake at Banda Aceh. This provides an insight to the frequency distribution of the ground shaking and is an important parameter for engineering applications. We see a strong peak in the acceleration response around 4- to 4.5-sec period, which is expected to have little effect on low-rise to intermediate-rise buildings. In addition, spectral accelerations are large for frequencies below 1 Hz, indicating that a significant amount of the shaking effects occurred at frequencies at which building damage can be expected in Banda Aceh.

Discussion

Strong ground motion simulations provide a powerful tool for studying the ground motions caused by earthquakes with few strong-motion recordings. This can give information on the extent and duration of strong shaking and, in cases where the effects of local geology are known, also provide estimates of the absolute ground shaking levels. In this respect, the present study can help in distinguishing the regions, which were significantly damaged by the earthquake shaking before the tsunami hit during the 26 Decem-

ber 2004 earthquake. According to our results, the most affected areas are the islands along the subduction zone, which are situated directly above the ruptured fault segment, and the northwesternmost part of Sumatra. Though adding the effects of local geology will increase the extent of the affected area, we do not expect strong shaking at distances more than a few hundred kilometers from the ruptured fault plane.

In this study we conducted a retrospective analysis of the strong ground motion distribution associated with the 26 December 2004 Sumatra–Andaman earthquake. The input source parameters are obtained from various studies of the earthquake and are expected to be a good representation of the earthquake source. However, uncertainties are present in the input parameters. A detailed analysis of the effect of varying input source parameters on the simulated ground motions has been performed by Sørensen *et al.* (unpublished manuscript, 2006) for the Istanbul area, Turkey. Results from this study show that the variation in ground-motion values is strongly frequency dependent and that the velocity spectrum is the most stable ground-motion measure. To incorporate the uncertainties related to rise time and rupture velocity in the present study, these parameters have been randomized within bounds representing the minimum and maximum values. Using different randomizations causes changes in the peak ground-motion values of up to 10%–20%. This is relatively stable in comparison to the variation observed by changing these parameters (up to 100%) (Sørensen *et al.*, unpublished manuscript, 2006).

One of the advantages of kinematic broadband ground-motion simulation is in its predictive capacity for the ground motions caused by future earthquakes. Such appli-

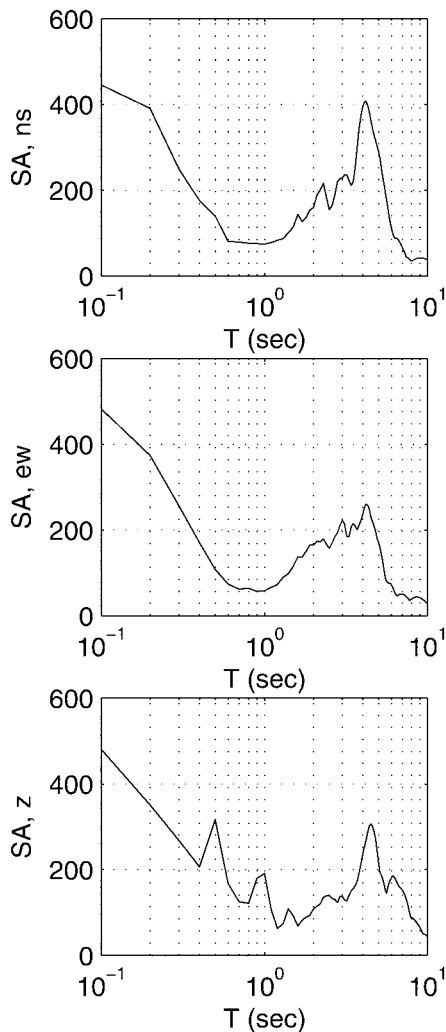


Figure 11. Pseudoacceleration response spectra with 5% damping for the 26 December 2004 earthquake at Banda Aceh (see Figs. 1 and 3 for location of the site).

cations are already conducted for areas where significant future seismic hazard is estimated. A recent example is the case of Istanbul, Turkey, where the predictive capacity of the methodology applied in this article is demonstrated (Pulido *et al.*, 2004). Despite the uncertainties in obtaining the correct source rupture parameters for future earthquakes, the simulated ground motions provide important clues for decision makers and engineers working in earthquake risk mitigation (Sørensen *et al.*, unpublished manuscript, 2006). It is desirable that similar studies are initiated for the Sumatra region, bearing in mind the continued earthquake threat in the region. Increased likelihood of further destructive earthquakes was predicted by the Coulomb stress modeling of McCloskey *et al.* (2005). Similar calculations performed for optimally oriented strike-slip faults have shown that the stresses have increased in the region near the Great Sumatran fault that may therefore have been brought closer to rupture (McCloskey *et al.*, 2006). This fault has historically expe-

rienced earthquakes up to $M 7.7$ and is probably capable of generating events with magnitude up to 7.9 (Petersen *et al.*, 2004). Such an earthquake, striking the northern part of Sumatra, could have disastrous consequences in an area already severely affected by the strong earthquake shaking and tsunami wave. We therefore recommend that research focusing on the likely occurrence of earthquakes in this region in the future should be given a priority.

Conclusions

In the present study we have used a hybrid procedure for modeling the ground motions caused by the 26 December 2004 Sumatra earthquake. The following conclusions can be drawn from the simulation results:

1. The maximum bedrock ground motions are at the order of 200 cm/sec (PGV) and 1200 cm/sec² (PGA), respectively, and occur off the coast of northern Sumatra and on the Nicobar islands.
2. Ground shaking has played a significant role in the destruction of northern Sumatra and the offshore islands before the tsunami hit these regions.
3. A comparison of the simulated waveforms to recorded velocity waveforms and spectra at the PPI station of the JISNET network shows in general a good agreement. Differences in waveform amplitudes may be due to local site effects at the recording site and the assumption of a 1D velocity model for our simulations, whereas the difference in spectral amplitudes can be explained by the simplified geometrical spreading function used or the lack of scattering in the simulation methodology.
4. Bedrock velocities in Banda Aceh reached values of 60 cm/sec. Assuming local site effects causing amplifications at the order of a factor of 1.5–2, this may explain shaking intensities up to IX, as observed by eyewitnesses and a field survey.

Acknowledgments

We would like to thank Dr. Hiroaki Negishi of the National Research Institute for Earth Science and Disaster Prevention (NIED), Japan, for providing the waveforms of the Sumatra earthquake recorded at the PPI station, JISNET (Japan-Indonesia broadband Seismic Network), operated by NIED. Many of the figures were created using the Generic Mapping Tools (GMT) software (Wessel and Smith, 1998).

References

- Ammon, C. J., C. Ji, H.-K. Thio, D. Robinson, S. Ni, V. Hjorleifsdottir, H. Kanamori, T. Lay, S. Das, D. Helmberger, G. Ichinose, J. Polet, and D. Wald (2005). Rupture process of the 2004 Sumatra–Andaman earthquake, *Science* **308**, 1133–1139.
- Atkinson, G. M., and D. M. Boore (1995). Ground motion relations for eastern North America, *Bull. Seism. Soc. Am.* **85**, 17–30.
- Banghar, A. R. (1987). Seismo-tectonics of the Andaman-Nicobar islands, *Tectonophysics* **133**, 97–107.

- Bilham, R. (2005). A flying start, then a slow slip, *Science* **308**, 1126–1127.
- Boore, D. M. (2003). Simulation of ground motion using the stochastic method, *Pure Applied Geophysics* **160**, 635–676.
- Boore, D. M., W. Joyner, and T. Fumal (1997). Equations for estimating horizontal response spectra and peak accelerations from western North American earthquakes: a summary of recent works, *Seism. Res. Lett.* **68**, 128–153.
- Bouchon, M. (1981). A simple method to calculate Green's functions for elastic layered media, *Bull. Seism. Soc. Am.* **71**, 959–971.
- Brune, J. (1970). Tectonic stress and the spectra of seismic shear waves from earthquakes, *J. Geophys. Res.* **75**, 4997–5009.
- Campbell, K. (1997). Empirical near-source attenuation relationships for horizontal and vertical components of peak ground acceleration, peak ground velocity and pseudo-absolute acceleration response spectra, *Seism. Res. Lett.* **68**, 154–179.
- Das, S., and B. V. Kostrov (1986). Fracture of a single asperity on a finite fault: a model for weak earthquakes? in S. Das, J. Boatwright, and C. Scholz (Editors), *Earthquake Source Mechanism*, American Geophysical Union, Washington, D.C. 91–96.
- Eguchi, T., S. Uyeda, and T. Maki (1979). Seismotectonics of the Andaman Sea, *Tectonophysics* **57**, 35–51.
- Glimsdal, S., G. K. Pedersen, K. Atakan, C. Harbitz, and H. P. Langtangen (2006). Propagation of the Dec. 26, 2004 Indian Ocean Tsunami: effects of dispersion and source characteristics, *J. Fluid Mech. Res.* **33**, no. 1, 15–43.
- Global Centroid Moment Tensor (CMT) Project catalog search, www.globalcmt.org/CMTsearch.html (last accessed November 2006).
- Honda, R., Y. Takahashi, M. H. Pradono, and R. Kurniawan (2005). Earthquake damage survey and observed intensities during the 2004 Sumatra earthquake www.catfish.dpri.kyoto-u.ac.jp/~honda/aceh2004/ (in Japanese) (last accessed May 2006).
- Intergovernmental Oceanographic Commission (IOC), International Hydrographic Organisation (IHO), and British Oceanographic Data Centre (BODC) (2003). *Centenary Edition of the GEBCO Digital Atlas*, Intergovernmental Oceanographic Commission and the International Hydrographic Organization as part of the General Bathymetric Chart of the Oceans, British Oceanographic Data Centre, Liverpool, U.K. (CD-ROM).
- Irikura, K. (1986). Prediction of strong acceleration motion using empirical Green's function, *Proc. 7th Japan. Earthq. Eng. Symp.*, 151–156.
- Ishida, M., S. Maruyama, D. Suetsugu, S. Matsuzaka, and T. Eguchi (1999). Superplume project: towards a new view of whole earth dynamics, *Earth Planets Space* **51**, no. 1, 1–5.
- Ji, C. (2005). Preliminary rupture model of the December 26, 2004 Sumatra earthquake, http://neic.usgs.gov/neis/eq_depot/2004/eq_041226/neic_slav_ff.html (last accessed January 2006).
- Khan, S. A., and Ó. Gudmundsson (2005). GPS Analyses of the Sumatra–Andaman earthquake, *EOS* **88**, 89.
- Lay, T., H. Kanamori, C. Ammon, M. Nettles, S. N. Ward, R. C. Aster, S. L. Beck, S. L. Bilek, M. R. Brudzinski, R. Butler, H. R. DeShon, G. Ekström, K. Satake, and S. Sipkin (2005). The great Sumatra–Andaman earthquake of December 26, 2004, *Science* **308**, 1127–1133.
- Masturyono, R. McCaffrey, D. A. Wark, S. W. Roecker, Fauzi, G. Ibrahim, and Sukhyar (2001). Distribution of magma beneath the Toba caldera complex, north Sumatra, Indonesia, constrained by three-dimensional P wave velocities, seismicity, and gravity data, *Geochem. Geophys. Geosystems* **2**, 2000GC000096.
- McCaffrey, R., P. C. Zwick, Y. Bock, L. Prawiradirdjo, J. F. Genrich, C. W. Stevens, S. S. O. Puntodewo, and C. Subarya (2000). Strain partitioning during oblique plate convergence in northern Sumatra: geodetic and seismologic constraints and numerical modeling, *J. Geophys. Res.* **105**, no. B12, 28,363–28,376.
- McCloskey, J., S. S. Nalbant, and S. Stacy (2005). Earthquake risk from co-seismic stress, *Nature* **434**, 291.
- McCloskey, J., S. S. Nalbant, S. Stacey, and A. Antonioli (2006). Updated Earthquake Hazard in Sumatra, EGU General Assembly, Vienna, Austria, April 2006, abstract no. EGU06-A-10222.
- Midorikawa, S. (1993). Preliminary analysis for attenuation of peak ground velocity at a stiff site, in *Proc. International Workshop on Strong Motion Data*, Menlo Park, California, 13–17 December, vol. 2, U.S. Geological Survey, Menlo Park, California, pp. 39–48.
- Murphy, J. R., and L. J. O'Brien (1977). The correlation of peak ground acceleration amplitude with seismic intensity and other physical parameters, *Bull. Seism. Soc. Am.* **67**, 877–915.
- Newmark, N. M., and W. J. Hall (1982). *Earthquake Spectra and Design*, Earthquake Engineering Research Institute, Berkeley, California, 103 pp.
- Ortiz, M., and R. Bilham (2003). Source area and rupture parameters of the 31 December 1881 Mw = 7.9 Car Nicobar earthquake estimated from tsunamis recorded in the Bay of Bengal, *J. Geophys. Res.* **108**, no. B4, 2215–2229.
- Park, J., K. Anderson, R. Aster, R. Butler, T. Lay, and D. Simpson (2005). Global Seismographic Network records the great Sumatra–Andaman earthquake, *EOS* **86**, no. 6, 57–64.
- Petersen, M. D., J. Dewey, S. Hartzell, C. Mueller, S. Harmsen, A. D. Frankel, and K. Rukstales (2004). Probabilistic seismic hazard analysis for Sumatra, Indonesia and across the Southern Malaysian Peninsula, *Tectonophysics* **390**, 141–158.
- Prawiradirdjo, L., Y. Bock, R. McCaffrey, J. Genrich, E. Calais, C. Stevens, S. S. O. Puntodewo, C. Subarya, J. Rais, P. Zwick, and P. Fauzi (1997). Geodetic observations of interseismic strain segmentation at the Sumatra subduction zone, *Geophys. Res. Lett.* **24**, no. 21, 2601–2604.
- Pulido, N., and T. Kubo (2004). Near-fault strong motion complexity of the 2000 Tottori earthquake (Japan) from a broadband source asperity model, *Tectonophysics* **390**, 177–192.
- Pulido, N., A. Ojeda, K. Atakan, and T. Kubo (2004). Strong ground motion estimation in the Marmara Sea region (Turkey) based on a scenario earthquake, *Tectonophysics* **391**, 357–374.
- Si, H., and S. Midorikawa (2000). New attenuation relations for peak ground acceleration and velocity considering effects of fault type and site conditions, in *Proc. Twelfth World Conference on Earthquake Engineering*, Auckland, New Zealand, 30 January–4 February 2000, paper no. 0532.
- Simoës, M., J. P. Avouac, R. Cattin, and P. Henry (2004). The Sumatra subduction zone: a case for a locked fault zone extending into mantle, *J. Geophys. Res.* **109**, no. B 10402, 16 pp.
- Singh, S. K., R. S. Dattatrayam, G. Suresh, A. Iglesias, B. K. Bansal, X. Peres, M. Ordaz, H. K. Gupta, P. R. Baidya, J. L. Gautam, G. Kumar, and R. K. Singh (2005). The Great Sumatra–Andaman Earthquake of 2004: regional broadband seismograms from India, *Seism. Res. Lett.* **76**, no. 6, 684–692.
- Sørensen, M. B., I. Oprsal, S. Bonnefoy-Claudet, K. Atakan, P. M. Mai, N. Pulido, and C. Yalciner (2006). Local site effects in Ataköy, Istanbul, Turkey, due to a future large earthquake in the Marmara Sea, *Geophys. J. Int.* (in press).
- Stein, S., and E. A. Okal (2005). Speed and size of the Sumatra earthquake, *Nature* **434**, 581–582.
- Wald, D. J., V. Quitoriano, T. H. Heaton, and H. Kanamori (1999). Relationships between peak ground acceleration, peak ground velocity and modified Mercalli intensity in California, *Earthquake Spectra* **15**, 557–564.
- Wessel, P., and W. H. F. Smith (1998). New improved version of Generic Mapping Tools released, *EOS* **79**, 579.
- Yagi, Y. (2004). Preliminary results of rupture process for 2004 off coast of Northern Sumatra giant earthquake, <http://iisee.kenken.go.jp/staff/yagi/eq/Sumatra2004/Sumatra2004.html> (last accessed May 2006).
- Yamanaka, Y. (2005). Source rupture process of the Dec. 26, 2004 Sumatra–Andaman earthquake, EIC Seismological Note No. 161, ERI, University of Tokyo, Japan, available at www.eri.u-tokyo.ac.jp/

sanchu/Seismo_Note/2004/EIC161e.html (last accessed January 2006).

Youngs, R. R., S.-J. Chiou, W. J. Silva, and J. R. Humphrey (1997). Strong ground motion attenuation relationships for subduction zone earthquakes, *Seism. Res. Lett.* **68**, no. 1, 58–73.

Department of Earth Science
Allegt. 41
5008 Bergen, Norway
kuvvet.atakan@geo.uib.no
(M.B.S., K.A.)

National Strong Motion Mapping Project
National Research Institute for Earth Science and Disaster Prevention
3-1 Tennodai, Tsukuba-shi, Ibaraki-ken, Japan 305-0006
nelson@bosai.go.jp
(N.P.)

Manuscript received 14 January 2006.